Macromolecules

Volume 29, Number 4 February 12, 1996

Reviews

Unifying Weak- and Strong-Segregation Block Copolymer Theories

M. W. Matsen* and F. S. Bates

Department of Chemical Engineering and Materials Science, University of Minnesota, Minneapolis, Minnesota 55455

Received August 3, 1995; Revised Manuscript Received November 8, 1995[⊗]

ABSTRACT: A mean-field phase diagram for conformationally symmetric diblock melts using the standard Gaussian polymer model is presented. Our calculation, which traverses the weak- to strong-segregation regimes, is free of traditional approximations. Regions of stability are determined for disordered (DIS) melts and for ordered structures including lamellae (L), hexagonally packed cylinders (H), body-centered cubic spheres ($Q_{Im\bar{3}m}$), close-packed spheres (CPS), and the bicontinuous cubic network with $Ia\bar{3}d$ symmetry ($Q_{Ia\bar{3}d}$). The CPS phase exists in narrow regions along the order−disorder transition for $\chi N \geq 17.67$. Results suggest that the $Q_{Ia\bar{3}d}$ phase is not stable above $\chi N \sim 60$. Along the L/$Q_{Ia\bar{3}d}$ phase boundaries, a hexagonally perforated lamellar (HPL) phase is found to be nearly stable. Our results for the bicontinuous $Pn\bar{3}m$ cubic ($Q_{Pn\bar{3}m}$) phase, known as the OBDD, indicate that it is an unstable structure in diblock melts. Earlier approximation schemes used to examine mean-field behavior are reviewed, and comparisons are made with our more accurate calculation.

1. Introduction

AB block copolymer melts have received considerable attention because immiscibility between A and B blocks induces self-assembly into various ordered microstructures.[1,2] In the high-temperature disordered (DIS) phase, A and B blocks mix homogeneously, but as the temperature is lowered (i.e., the Flory-Huggins χ parameter is increased), they separate on a microscopic scale forming A- and B-rich domains separated by an extensive amount of internal interface. Various geometries of these domains occur depending, to a large degree, on the spontaneous mean curvature of the internal interface, which is produced by a mismatch in entropic stretching energy of the A and B blocks.[1,3] The classical structures are lamellae (L), hexagonally packed cylinders (H), and a body-centered cubic (bcc) array of spheres ($Q_{Im\bar{3}m}$). Although early results suggested both $Q_{Im\bar{3}m}$[4] and close-packed spheres (CPS),[5] the latter is no longer accepted as an equilibrium structure. (CPS refers to either face-centered cubic (fcc) or hexagonally close-packed (hcp).) The first nonclassical phase was observed in 1972[6] and identified in 1986 by Thomas *et al.*[7] as a bicontinuous cubic structure ($Q_{Pn\bar{3}m}$) with $Pn\bar{3}m$ symmetry, often referred to as the ordered bicontinuous double-diamond (OBDD) phase. Just two years ago, there emerged evidence for a second bicontinuous structure ($Q_{Ia\bar{3}d}$), this time with $Ia\bar{3}d$ symmetry, sometimes referred to as the gyroid phase.[8,9] At about the same time, evidence was presented for a stable hexagonally perforated lamellar (HPL) phase, sometimes called catenoid lamellar, where each of the thinner minority-component lamellae is covered by a hexagonal arrangement of perforations.[10−12] Experiments also suggested a hexagonally modulated lamellar (HML) phase where the perforations are not fully developed,[10] but it is uncertain whether this is an equilibrium phase. The latest development has been a growing skepticism in regard to the $Q_{Pn\bar{3}m}$ phase. Initially, it was realized that samples identified as $Q_{Pn\bar{3}m}$ by a characteristic "wagon-

[⊗] Abstract published in *Advance ACS Abstracts*, January 1, 1996.

0024-9297/96/2229-1091$12.00/0

wheel" TEM image[6,7,13,14] could be in error because the $Q_{Ia\bar{3}d}$ phase produces an analogous image.[8,11,12] This stressed that scattering methods were important in order to determine the symmetry of a bicontinuous phase, motivating the reexamination of such samples. Indeed, closer examination of samples originally identified as $Q_{Pn\bar{3}m}$ showed them to be $Q_{Ia\bar{3}d}$.[15] As of yet, compelling evidence using advanced scattering techniques does not exist for the $Q_{Pn\bar{3}m}$ phase.

In general, the theoretical study of diblock copolymer melts has been based upon a single, standard, Gaussian model.[3,16-56] In this model, each molecule of the melt is composed of N segments of which a fraction f forms the A block and the rest forms the B block. For convenience, A and B segments are usually defined to have equal volumes. In addition, the "coarse-grained" segments each represent a sufficient length of polymer such that they can be treated as Gaussian where internal conformational states of the segments produce a Hookian entropic penalty of stretching. The statistical length, a, of a segment is its average RMS end-to-end length when no tension is applied and is related to the effective spring constant. Most calculations examine the conformationally symmetric case where the A and B statistical segment lengths are equal. The model accounts for hard-core repulsive interactions by implementing an incompressibility constraint where the average segment concentration is forced to be uniform. The remaining interactions are assumed to be local and are treated by the enthalpy term, $k_BT\chi\rho_0\int\phi_A(\mathbf{r})\phi_B(\mathbf{r})\,d\mathbf{r}$, where $\phi_A(\mathbf{r})$ and $\phi_B(\mathbf{r})$ are the volume fractions of A and B segments, respectively, at position $\mathbf{r}$ and ρ_0 is the segment density. This simplified model for block copolymer melts retains the three most important ingredients: entropic chain stretching, incompressibility, and immiscibility between unlike segments. Of course, there are possible refinements which we discuss below.

2. Approximations to Mean-Field Theory

The thermodynamics of even the simplified standard model cannot be determined exactly. Treating molecular correlations in the melt represents a formidable problem, and so most calculations resort to the mean-field approximation. The self-consistent field theory (SCFT) for this was developed by Helfand and coworkers in a series of papers beginning in 1971.[16-19] We note that Scheutjens and Fleer[57] developed an analogous lattice-based SCFT; however, due to the geometric constraints associated with a lattice, it is not well suited for dealing with the nonlamellar structures exhibited by block copolymers. As we discuss later, the mean-field approximation works well for high molecular weight polymers. Equally important is that the fluctuation corrections to it are well understood. Still, at the time of its introduction, the full SCFT represented a computationally difficult problem and so numerous additional approximations were implemented. Most of the theoretical approaches that followed used the standard model, mean-field theory, and differed only in regard to the approximations that were added to the SCFT. Some of the additional approximations simply introduced a degree of inaccuracy, while others restricted the validity of the calculation to, for example, weak or strong segregations. However, by combining results from the various approaches, the general behavior of the standard model has been revealed. Now with the development of theoretical methods and computer technology, we demonstrate that most of the mean-field phase diagram can be calculated without resorting to these additional approximations. In order to put the present calculation into the proper perspective, we briefly discuss the development of strategies for obtaining approximations to the phase diagram before presenting our more accurate diagram.

In the original work by Helfand and co-workers, two additional approximations were devised: a narrow-interface approximation (NIA)[16] and a unit-cell approximation (UCA).[17] The NIA was implemented to solve the statistical mechanics of a block copolymer in the presence of a steplike potential (i.e., an internal interface). Although equations for the lamellar phase could then be solved, those for doubly- and triply-periodic structures were still unmanageable. To cope with the more complicated microstructures, the SCFT was supplemented with circular and spherical approximations for the Wigner–Seitz cells of the H and $Q_{Im\bar{3}m}$ phases, respectively. This produced inaccuracies by underestimating the free energies of these phases and also made the calculation insensitive to the equilibrium packing arrangement of the cylindrical and spherical units. For example, it could not distinguish between the $Q_{Im\bar{3}m}$ and CPS phases. Furthermore, the UCA could not straightforwardly be generalized to consider more complex phases. More significantly, the NIA restricted calculations to the strong-segregation regime (i.e., $\chi N \gg 10$). In 1980, Leibler[20] complimented this with a Landau expansion of the SCFT based on the random-phase approximation (RPA), providing results for the weak-segregation regime (i.e., $\chi N \sim 10$). This work also provided a free energy potential which could be mapped onto the Brazovskii Hamiltonian,[58] allowing for the first calculation that went beyond mean field and considered fluctuation effects.[21] In 1985, Semenov[22] introduced a strong-segregation theory (SST) for examining the zero-temperature (i.e., infinite χN) limit of the standard model. Notably, fluctuation effects become negligible in this limit, and thus mean field becomes exact. Still, Semenov implemented the UCA as well as a further approximation to deal with exclusion zones that occur in the H and $Q_{Im\bar{3}m}$ phases, and so his calculation did not provide exact zero-temperature results. Shortly after, Ohta and Kawasaki[23] presented a density-functional theory (DFT) based on the RPA that was significant because it could be applied to any degree of segregation. It is difficult to assess all the approximations in this DFT and others like it,[24-26] but a comparison[27] to the exact SCFT result[37] for the lamellar phase indicated that while DFT gives qualitatively correct results, it is quantitatively inaccurate. Likewise, comparing the infinite χN results of the DFT to those of the SST supported this conclusion.[25] Recently, Vavasour and Whitmore[28] demonstrated that the DFT was unnecessary. Using only the UCA, they evaluated the mean-field phase diagram from the weak- to the strong-segregation regime, bridging the RPA and SST. Because their calculation still implemented the UCA, it was restricted to the classical phases.

The first calculation to examine a complex phase[24] applied DFT to the $Q_{Pn\bar{3}m}$ phase and found it to be unstable at strong segregations. In addition to using the approximations involved in the Ohta–Kawasaki approach, this calculation did not minimize the free energy with respect to the shape of the internal interface, but rather assumed it was a constant mean-curvature (CMC) surface. Later, complex phases were

examined at weak segregations using the RPA. Because the original calculation of Leibler implemented a first-harmonic approximation for the segment profiles, it was insensitive to the free energy differences between phases with the same set of principal scattering vectors. Consequently, harmonic corrections had to be added to the Leibler theory in order to examine complex phases.[59] Doing so, Olvera de la Cruz, Mayes, and Swift[29] suggested that a bicontinuous HPL phase would be stable at weak segregations. A more recent calculation by Hamley and Bates[30] showed this phase was, in fact, unstable as were numerous other complex phases. About the same time, it was demonstrated that the full SCFT could be solved for any periodic phase while considering a large number of harmonics (i.e., Fourier components) and making no assumptions regarding the shape of the internal interface.[31] Although this calculation found the $Q_{Pn\bar{3}m}$ and HPL phases to be unstable, it predicted the $Q_{Ia\bar{3}d}$ phase to be stable for weak to intermediate segregations. Because this calculation was still limited in the number of Fourier components that could be used in representing the segment profiles, it could not be extended to the strong-segregation limit. Nevertheless, the calculation was able to provide suggestive results that the $Q_{Ia\bar{3}d}$ phase may extend to strong segregations in a narrow channel of nearly uniform width. According to SST calculations, the HPL,[32] $Q_{Pn\bar{3}m}$,[33,34] and $Q_{Ia\bar{3}d}$[33] phases are all unstable in the infinite χN limit. However, these SST calculations all ignore exclusion zones and make certain assumptions regarding the shape of the internal interfaces, and hence, they are not conclusive. Nevertheless, they strongly suggest that the $Q_{Ia\bar{3}d}$ region calculated in ref 31 terminates at finite χN, which would be consistent with recent experimental findings.[1,60] Earlier experiments,[6,7,13,14] performed with samples prepared by slow solvent casting, lead to the conclusion that channels of bicontinuous phase separate the H and L phases throughout the strong-segregation regime. Although this point remains controversial, we believe this reflects a metastable state. The rationale is that as a sample passes through the weak-segregation regime, the bicontinuous phase develops, the sample becomes kinetically trapped, and then it is unable to transform to the stable phase at strong segregations.

3. Full Mean-Field Theory

In this section, the standard model using the full SCFT is examined without any of the additional approximations discussed in the previous section. When possible, comparisons are made with those earlier calculations to show, for example, when the weak- and strong-segregation approximations are valid. We refer the reader to ref 31 for the details of how the full SCFT calculation is performed. The only difference between that calculation and the present one is that here far more Fourier terms are used to represent the segment profiles. This allows us to produce more accurate results and to extend the phase boundaries now unifying the weak- and strong-segregation block copolymer theories. The most significant prediction of the present calculation is that the $Q_{Ia\bar{3}d}$ regions pinch off as the strong-segregation regime is entered. Another notable result is that beyond the weak-segregation regime, the CPS phase is found to be stable in narrow regions along the order–disorder transition. The calculation also shows the HPL phase to be nearly stable, suggesting that it may actually become stable at strong segregations. On the other hand, the $Q_{Pn\bar{3}m}$ phase is found to be rather unstable, in agreement with recent suggestions that it is not an equilibrium phase in diblock melts.

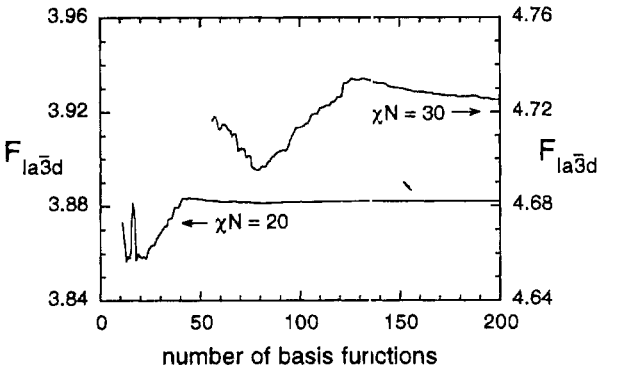

Figure 1. Convergence of the free energy of the $Q_{Ia\bar{3}d}$ phase per molecule in units of k_BT as the number of basis functions is increased. The left scale applies to the lower curve for $\chi N = 20$ and $f = 0.33$, and the one on the right applies to the upper curve for $\chi N = 30$ and $f = 0.33$.

Before discussing the results of the complete SCFT, we provide an intuitive explanation of how this calculation improves on earlier ones. The key to examining complex periodic phases centers around a basis function expansion of all spatially dependent quantities. For instance, the A-segment volume fraction is expanded as

$$\phi_A(\mathbf{r}) = \phi_{A,1}f_1(\mathbf{r}) + \phi_{A,2}f_2(\mathbf{r}) + \phi_{A,3}f_3(\mathbf{r}) + \dots \quad (1)$$

The self-consistent field equations are then transformed to Fourier space, and instead of solving the equations directly for $\phi_A(\mathbf{r})$ as in ref 28, the set of coefficients $\phi_{A,i}$ is solved for. The basis functions are selected such that they possess the symmetry of the phase being considered. For the $Q_{Ia\bar{3}d}$ phase,[61] the first few are

$$f_1(\mathbf{r}) = 1 \quad (2)$$

$$f_2(\mathbf{r}) = \sqrt{8/3}(\cos(X)\sin(Y)\sin(2Z) + \cos(Y)\sin(Z)\sin(2X) + \cos(Z)\sin(X)\sin(2Y)) \quad (3)$$

$$f_3(\mathbf{r}) = \sqrt{4/3}(\cos(2X)\cos(2Y) + \cos(2Y)\cos(2Z) + \cos(2Z)\cos(2X)) \quad (4)$$

$$f_4(\mathbf{r}) = \sqrt{4/3}(\sin(2X)[\cos(3Y)\sin(Z) - \sin(3Y)\cos(Z)] + \sin(2Y)[\cos(3Z)\sin(X) - \sin(3Z)\cos(X)] + \sin(2Z)[\cos(3X)\sin(Y) - \sin(3X)\cos(Y)]) \quad (5)$$

$$f_5(\mathbf{r}) = \sqrt{2/3}(\cos(4X) + \cos(4Y) + \cos(4Z)) \quad (6)$$

where $X \equiv 2\pi x/D$ is a dimensionless length, Y and Z are defined similarly, and D is the size of the cubic unit cell. The basis functions are ordered according to the magnitudes of their wavevectors. This sequence of functions is infinite and must be truncated in order to perform a numerical calculation. The more basis functions retained, the more accurate the calculation. Figure 1 shows $F_{Ia\bar{3}d}$, the free energy of the $Q_{Ia\bar{3}d}$ phase per molecule measured in units of k_BT, as a function of the number of basis functions for $\chi N = 20$ and 30 at $f = 0.33$. This figure demonstrates the need for more basis functions as the segregation increases, causing the width of the internal interface to become narrow relative to D. Locating a phase boundary at a given value of χN to an accuracy in f of $\pm 10^{-3}$ requires typically an

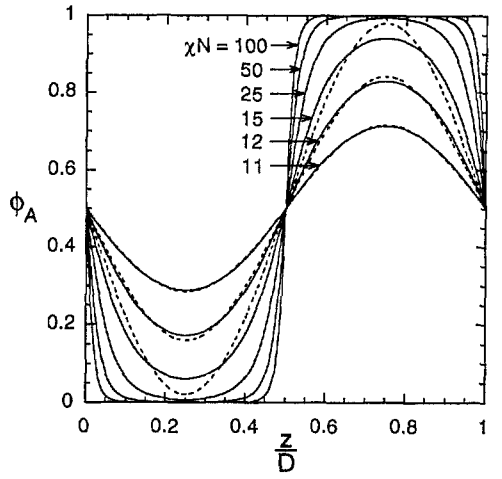

Figure 2. A-segment profiles over one period of the lamellar phase of a symmetric ($f = 0.5$) diblock melt for $\chi N = 11$, 12, 15, 25, 50, and 100. Dashed lines denote first-harmonic approximations for the profiles at $\chi N = 11$, 12, and 15.

accuracy of $\pm 10^{-4}$ in the free energies. We use a generous number of basis functions in order to be confident that we have attained convergence. For the $Q_{Ia\bar{3}d}$ phase, 175, 325, and 450 functions are used for $\chi N = 20$, 30, and 40, respectively. For comparison, the first-harmonic approximation used in the RPA calculation of Leibler retains just the first two basis functions, i.e., $f_1(\mathbf{r})$ and $f_2(\mathbf{r})$, for each phase. Furthermore, that calculation performs a power-series (i.e., Landau) expansion of the free energy potential in $\phi_{A,2}$ which is truncated after the fourth-order term. In the other extreme, the SST assumes $\phi_A(\mathbf{r})$ is a step function with values of either 0 or 1. It further assumes that copolymers are strongly stretched following straight paths, whereas the SCFT calculates distributions over all paths weighting them by the appropriate Boltzmann factors.

The product χN is the quantity that controls the degree of segregation between A and B blocks. Typically, segregation is categorized into three regimes: weak, intermediate, and strong. Because there are no well-defined criteria for separating these regimes, they are usually discussed in vague terms. Here, we present some results to better indicate over what intervals of χN these regions occur. As a representative example, we examine the lamellar phase of a symmetric ($f = 0.5$) diblock and plot the profile for the A-segment density $\phi_A(\mathbf{r})$ at several degrees of segregation in Figure 2. The weak-segregation regime occurs when the profile is sinusoidal or, in general, when the profile is well approximated by its first Fourier component. The dashed lines in Figure 2 show the first-harmonic approximation for the weaker segregated cases. Based on that, the weak to intermediate crossover occurs at $\chi N \sim 12$, not much above the mean-field critical point at $\chi N = 10.495$. Consequently, the RPA is only accurate in a narrow χN range as was demonstrated earlier in ref 28. The strong-segregation regime occurs when the middle of each domain becomes essentially pure. It is rather arbitrary as to what is meant by pure, but requiring $\phi_A(\mathbf{r}) > 0.9999$ in the middle of an A-rich domain provides a crossover from intermediate to strong segregation at $\chi N \sim 50$. The SST not only requires the A and B blocks to be strongly segregated, it also requires them to be strongly stretched and the internal interfaces to be narrow. As illustrated below, the SST does not become accurate for predicting domain spacings and

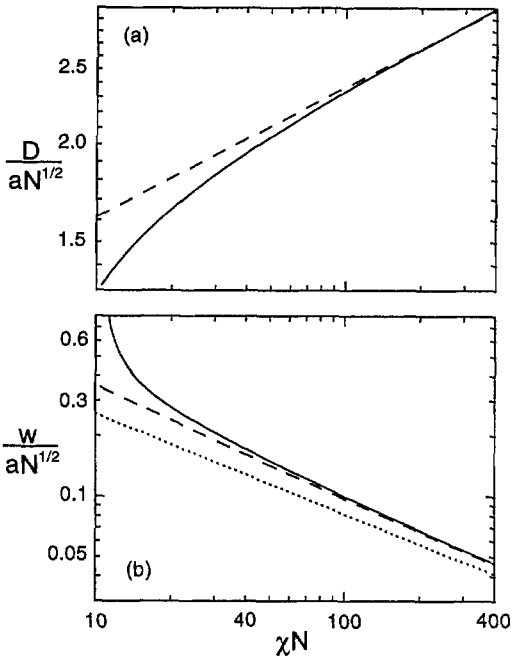

Figure 3. Period (a) and interfacial width (b) of the lamellar phase for a symmetric ($f = 0.5$) diblock melt plotted logarithmically as a function of χN. Solid lines are obtained from SCFT, dashed lines denote the SST predictions given by eqs 7 and 8, and the dotted line in (b) represents $w = 2a/(6\chi)^{1/2}$.

interfacial widths until $\chi N \sim 100$. In general, far larger degrees of segregation are required before the SST becomes reliable.[35]

Many interpret the segregation regimes on the basis of how the lamellar spacing, D, and the interfacial width, w, vary with N. Following a typical definition, we equate w to $(d\phi_A/dz)^{-1}$ evaluated at the interface. In Figure 3, these quantities are plotted logarithmically for both the SCFT and SST. In the DIS phase at $f = 0.5$, the characteristic length scale is $2\pi/q^* = 1.318aN^{1/2}$, where q^* is the wavevector at which the structure function attains its maximum.[20] This $N^{1/2}$ scaling should be associated with the absence of segregation.[37] Often it is assumed that this scaling continues into the weak-segregation regime. This confusion has been amplified by misleading DFC calculations,[25,26] which predicted a $N^{1/2}$ scaling for weakly ordered microstructures. This result has been attributed to neglecting the wavevector dependence in the high-order vertex functions of the RPA expansion.[27] The more accurate SCFT calculations[28,37] like the one presented here show that the exponent jumps immediately as the weak-segregation regime is entered, which occurs upon crossing the critical point. We find that the exponent jumps to 0.994, consistent with the RPA calculation in ref 36 and intermediate to the exponents quoted in refs 37 and 38. When fluctuations are taken into account, segregation begins in the DIS phase causing the exponent to increase prior to the order–disorder transition[39,62] consistent with experiment.[63] Fitting the weak to intermediate regimes, experiments[63,64] measure an exponent of $\sim 4/5$. At the strong segregations, D begins to scale with an exponent of $2/3$ consistent with experiment[13,65] and with the SST result[22,40]

$$\frac{D}{aN^{1/2}} = 2\left(\frac{8}{3\pi^4}\right)^{1/6}(\chi N)^{1/6} \qquad (7)$$

shown with a dashed line in Figure 3. We note that

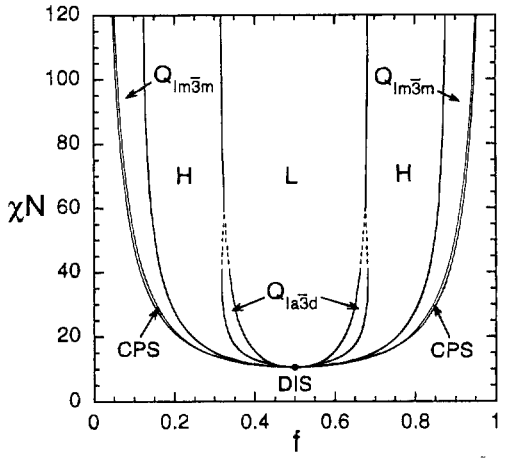

Figure 4. Mean-field phase diagram for conformationally symmetric diblock melts. Phase are labeled L (lamellar), H (hexagonal cylinders), $Q_{Ia\bar{3}d}$ (bicontinuous $Ia\bar{3}d$ cubic), $Q_{Im\bar{3}m}$ (bcc spheres), CPS (close-packed spheres), and DIS (disordered). Dashed lines denote extrapolated phase boundaries, and the dot denotes the mean-field critical point.

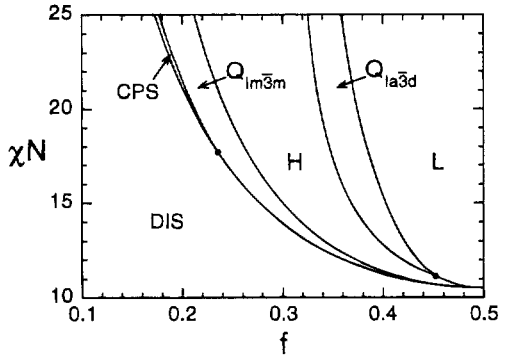

Figure 5. Expanded view of the phase diagram in Figure 4, showing the weak-segregation regime. The DIS + CPS + $Q_{Im\bar{3}m}$ and H + $Q_{Ia\bar{3}d}$ + L triple points are denoted with dots.

while DFT calculations also obtain this $^2/_3$ scaling, they inaccurately predict the proportionality constant.[23,25,26] At strong segregations, the interfacial width becomes independent of N and approaches $w = 2a/(6\chi)^{1/2}$. Because this approximation never becomes accurate for reasonable segregations,[37] Semenov[40] was stimulated to derive an improved SST-based expression

$$\frac{w}{aN^{1/2}} = \frac{2}{(6\chi N)^{1/2}}\left[1 + \frac{4}{\pi}\left(\frac{3}{\pi^2\chi N}\right)^{1/3}\right] \qquad (8)$$

which provides an accurate estimation of w by $\chi N \sim 100$. We note that refs 40 and 41 illustrated that fluctuations have a significant effect on w and that they need to be accounted for when comparing theory to experiment.

Figure 4 presents the SCFT phase diagram for χN up to 120. In agreement with a prediction by Semenov,[42] there are narrow regions of stability along the order–disorder transition for the CPS phase, extending toward the strong-segregation limit from DIS + CPS + $Q_{Im\bar{3}m}$ triple points at $\chi N = 17.67$ and $f = 1 - f = 0.235$ (see Figure 5). We note that while the regions of stability for the classical ordered phases L, H, and $Q_{Im\bar{3}m}$ grow with increasing χN, the region of stability for the bicontinuous $Q_{Ia\bar{3}d}$ phase decreases monotonically beyond $\chi N \sim 18$ where its width is $\Delta f = 0.037$. Initially, it narrows gradually, but this becomes more rapid as χN increases. Table 1 lists coordinates for the $Q_{Ia\bar{3}d}$ phase boundaries, which originate from triple points at

Table 1. Coordinates along the Boundaries of the $Q_{Ia\bar{3}d}$ Phase[a]

χN	$f_{H/Q}$	q^*_H/q^*_Q	$f_{Q/L}$	q^*_Q/q^*_L	Δf	$\Delta F_{Pn\bar{3}m}$	ΔF_{HPL}
40	0.318		0.337		0.019		
35	0.318	1.028	0.343	1.033	0.025	0.0388	0.0084
30	0.320	1.026	0.349	1.030	0.029	0.0345	0.0076
26	0.324	1.023	0.356	1.025	0.032	0.0299	0.0069
24	0.327	1.021	0.361	1.022	0.034	0.0272	0.0065
22	0.332	1.020	0.367	1.018	0.036	0.0245	0.0059
20	0.338	1.018	0.375	1.015	0.037	0.0213	0.0050
18	0.346	1.016	0.384	1.009	0.037	0.0179	0.0040
16	0.359	1.015	0.396	1.001	0.036	0.0141	0.0030
14	0.380	1.013	0.411	0.995	0.031	0.0097	0.0019
12	0.419	1.011	0.434	0.990	0.015	0.0060	0.0007

[a] Also listed are the ratios of q^*, the magnitude of the principal scattering vector, for the two equilibrium phases along each transition. (The subscript Q denotes $Q_{Ia\bar{3}d}$.) The last two columns list the excess free energy per molecule in units of k_BT for the $Q_{Pn\bar{3}m}$ and HPL phases along the H/$Q_{Ia\bar{3}d}$ and $Q_{Ia\bar{3}d}$/L transitions, respectively.

$\chi N = 11.14$ and $f = 1 - f = 0.452$ (see Figure 5). The fourth column demonstrates the narrowing of the $Q_{Ia\bar{3}d}$ channel, suggestive of an impending H + $Q_{Ia\bar{3}d}$ + L triple point beyond which the $Q_{Ia\bar{3}d}$ phase would be unstable. At $\chi N = 40$, where the width is only $\Delta f = 0.019$, 450 basis functions are used to evaluate the free energy of the $Q_{Ia\bar{3}d}$ phase. Although the large number of basis functions becomes prohibitive, we are prevented from extending these transitions further due to convergence problems in solving the self-consistent field equations. We attribute this problem to the Fourier series representation of the segment profiles, because small displacements in a sharp interface can produce drastic changes in large wavevector Fourier components. This seems to be particularly problematic for the $Q_{Ia\bar{3}d}$ phase. Still, the width of the $Q_{Ia\bar{3}d}$ region must vary continuously and thus become even narrower beyond $\chi N = 40$, almost certainly pinching off. If this was not to happen, it would require the trends that have slowly and monotonically developed to make an unprecedented and unphysical reversal. Although we cannot absolutely say the $Q_{Ia\bar{3}d}$ phase pinches off, it seems highly likely that it does, and the SST calculation[33] supports this conclusion. We note that, at weak segregations, both the CPS and the $Q_{Ia\bar{3}d}$ phase pinch off prior to the mean-field critical point as illustrated in Figure 5, because their principal scattering vectors do not form an octahedron.[20,66]

For the classical phases, calculations can be extended into the strong-segregation regime. In Figure 4, extrapolations are made for the $Q_{Ia\bar{3}d}$ phase boundaries, which have them terminating at $\chi N \sim 60$. Then, the remaining transitions are calculated up to $\chi N = 120$. Coordinates along the transitions between classical phases are listed in Table 2. As χN diverges, the DIS/CPS and CPS/$Q_{Im\bar{3}m}$ transitions will continue to approach $f = 0$ and 1. The infinite χN limit of the $Q_{Im\bar{3}m}$/H and H/L transitions can in principle be determined with the SST. Implementing the unit-cell approximation and ignoring the effect of exclusion zones, SST predicts the limits to be $f = 1 - f = 0.117$ and 0.299, respectively.[33,43] Proper treatments of the exclusion zones[44] demonstrate that they can be safely ignored,[33,34] and the error associated with the unit-cell approximation has been estimated for the L/H transition. Fredrickson[45] found that the UCA causes a ~4% shift, suggesting the correct L/H limit is at 0.287, while Likhtman and Semenov[34] predicted it at 0.293. However, SCFT results extrapolated to $\chi N = \infty$ provide compelling evidence that the

Table 2. Coordinates along the Boundaries between the Classical Phases[a]

χN	$f_{D/C}$	q^*_D/q^*_C	$f_{C/Q}$	q^*_C/q^*_Q	$f_{Q/H}$	q^*_Q/q^*_H	$f_{H/L}$	q^*_H/q^*_L
120	0.047		0.049	0.971	0.123	1.086	0.317	1.085
100	0.055		0.057	0.971	0.126	1.084	0.318	1.083
80	0.066	1.549	0.068	0.971	0.131	1.078	0.320	1.080
60	0.083	1.387	0.086	0.971	0.142	1.068	0.324	1.076
50	0.097	1.315	0.101	0.971	0.151	1.060	0.326	1.073
40	0.116	1.238	0.121	0.971	0.166	1.049	0.331	1.068
30	0.148	1.163	0.153	0.970	0.192	1.033	0.340	1.058
20	0.210	1.095	0.212	0.968	0.243	1.012	0.363	1.035

[a] Also provided are the ratios of q^*, the magnitudes of the principal scattering vectors. (The subscripts D, C, and Q denote DIS, CPS, and $Q_{Im\bar{3}m}$, respectively.)

Table 3. Scattering Amplitudes for the $Q_{Ia\bar{3}d}$ Phase at Various Coordinates, (χN, f)[a]

peak	(15,0.33)	(20,0.33)	(30,0.33)	(20,0.30)	(20,0.36)
(211)	1.0000	1.0000	1.0000	1.0000	1.0000
(220)	0.0919	0.1150	0.1274	0.1024	0.1286
(321)	0.0004	0.0003	0.0010	0.0002	0.0015
(400)	0.0020	0.0003	0.0002	0.0026	0.0002
(420)	0.0081	0.0057	0.0052	0.0145	0.0009
(332)	0.0058	0.0034	0.0032	0.0113	0.0002
(422)	0.0021	0.0022	0.0029	0.0046	0.0006
(431)	0.0011	0.0017	0.0026	0.0029	0.0007
(521)	0.0010	0.0019	0.0024	0.0022	0.0014
(440)	0.0006	0.0012	0.0019	0.0013	0.0009

[a] Peaks are identified with the standard spectroscopic (*hkl*) notation,[61] and amplitudes are normalized to the principal (211) peak.

true L/H limit is 0.310,[46] implying a significant and, as of yet, unidentified error in the SST. We note that DFT calculations are rather inaccurate, predicting 0.215 and 0.355 in ref 23 and 0.195 and 0.345 in ref 25 for the two infinite χN limits.

In addition to those phases found to be stable, we have examined the bicontinuous cubic phase with $Pn\bar{3}m$ symmetry and the hexagonally perforated lamellar phase up to $\chi N = 35$. Notably, both are predicted to be stable at certain compositions in diblock/homopolymer blends.[47] Here, we find that the $Q_{Pn\bar{3}m}$ phase is rather unstable but that the HPL phase is nearly stable. The $Q_{Pn\bar{3}m}$ phase is least unstable along the H/$Q_{Ia\bar{3}d}$ transition. In the seventh column of Table 1, its excess free energy $\Delta F_{Pn\bar{3}m}$ per molecule in units of k_BT is given for various values of χN along this transition. This energy increases monotonically with χN, and considering the two SST calculations,[33,34] the $Q_{Pn\bar{3}m}$ phase likely remains unstable as χN diverges. Along the L/$Q_{Ia\bar{3}d}$ transition, we find the excess free energy of the HPL phase, ΔF_{HPL}, to be quite small. Column eight in Table 1 shows that its excess free energy increases slowly with χN, suggesting that the HPL remains unstable into the strong-segregation limit in agreement with the SST calculation in ref 32. However, the possible stability of this phase should not be dismissed even in the infinite χN limit. The SST calculation assumed the perforations were aligned between adjacent minority-component layers. Both theoretical[31] and experimental[10,11,67] results suggest that it is more favorable to have the perforations staggered, and so the SST calculation probably overestimated its free energy. We note that preliminary work has indicated that introduction of conformational asymmetry may be sufficient to bring about the stability of the HPL phase at degrees of segregation accessible to our calculation. Because structures considered in the SCFT calculation have to be specified *a priori*, it is conceivable that other phases unknown to us could be stable. If this is so, we will likely learn of them through future experiments.

Neither the HPL or the CPS phase has a uniquely defined morphology. For the HPL phase, we examined the two geometries where the perforated minority-component layers are staggered in abab... and abcabc... sequences, and for the CPS phase, we examined both hcp and fcc structures. Not surprisingly, we find that both HPL structures provide the same spacings between lamellae and between perforations within the layers. Likewise, both CPS structures produce spacings between nearest-neighbor spheres that are indistinguishable. At strong segregations, we find the different packing arrangements in each case to be essentially degenerate in free energy. Because the basis function expansion converges more rapidly for the abcabc... stacking of perforated lamellae and for the fcc arrangement of spheres, those are the structures we use for most of our calculations involving the HPL and CPS phases, respectively. At weaker segregations, however, noticeable differences do exist, with the HPL phase slightly favoring the abab... sequence and the CPS phase favoring the hcp arrangement. Consequently, the hcp lattice must be used in order to accurately obtain the DIS + CPS + $Q_{Im\bar{3}m}$ triple points. Nevertheless, we expect that, in real melts, the slight differences in energies will be irrelevant in comparison to nonequilibrium effects and that the arrangement of either perforated lamellae or close-packed spheres will be random.

This paper has focused on equilibrium phase behavior, and to do so, all that was required was the free energy of each structure. The SCFT also predicts numerous other quantities, many of which can be tested against experiment. For example, the Fourier series representation of the segment profile, $\phi_A(\mathbf{r})$, straightforwardly yields scattering amplitudes.[3] For the $Q_{Ia\bar{3}d}$ phase at $\chi N = 20$ and $f = 0.33$, the Fourier coefficients $\phi_{A,i}$ for $i = 1, 2, 3, \ldots$ are 0.3300, 0.3164, −0.1074, 0.0050, −0.0057, ... The scattering amplitudes in Table 3 are obtained by squaring these coefficients. Notably, the theory predicts the (220) peak to be ~10% of the principal (211) peak in agreement with experiment.[8,15] Furthermore, the amplitudes for (321) and (400), the third and fourth reflections, respectively, are often abnormally small, consistent with measurements in refs 8, 11, and 15. Also provided by the theory are the magnitudes of the principal scattering vectors q^*.[68] Tables 1 and 2 provide the ratio of these magnitudes for the two equilibrium phases along each transition. For the DIS phase, q^* is taken to be the wavevector for which the structure function attains its maximum. For the CPS phase, we evaluate q^* using the fcc lattice; using the hcp lattice with the same spacing between spheres would reduce it by a factor of $8^{1/2}/3$. At strong segregations, q^* can exhibit discontinuities of several percent across order−order phase boundaries and much larger discontinuities across the order−disorder transition. At weak segregations, the discontinuities in q^* tend to become vanishingly small. Notably, the epitaxial growth of the $Q_{Ia\bar{3}d}$ phase[9,11] and of the $Q_{Im\bar{3}m}$ phase[69] from the H phase both imply small discontinuities in q^* consistent with the SCFT predictions. Additional information provided by the SCFT includes all the segment distribution functions.[41] For instance, the distribution of the ends or the junctions of the diblocks can be determined. From the A-segment profile, the width of the interfaces can be calculated as can the

detailed shape of the interface. Furthermore, the energy contributions due to the entropic stretching of the A and B blocks and due to the tension of the internal interface can be evaluated. We are currently pursuing such calculations, with the hope they will yield an explanation for what stabilizes the $Q_{Ia\bar{3}d}$ phase.

4. Discussion

Theory has now reached the stage where the mean-field phase diagram of the standard model is well-known for what is considered the most fundamental block copolymer system, the conformationally symmetric diblock melt. Several challenges remain, such as providing more conclusive evidence that the $Q_{Ia\bar{3}d}$ region closes off and accurately determining the resulting triple point. As we have discussed, pushing the present calculation to sufficient segregation will be rather difficult. Conceivably, it is possible to improve on the SST calculations making fewer assumptions regarding the shape of the internal interfaces and adding finite-segregation corrections. Although this may provide more convincing evidence that the $Q_{Ia\bar{3}d}$ is unstable at strong segregations, it is unlikely to accurately locate the triple point if it is indeed close to $\chi N \sim 60$. Of course, one issue this type of theory can never resolve is whether all the stable structures have been considered. This is where theory and experiment should be used in conjunction with each other. Experiments may detect stable or metastable states and provide clues to their structure. With that it may be possible to narrow the field of candidates and determine a new stable phase.

In the study of the standard model, perhaps the last task in regard to bulk phase behavior is to include fluctuation effects into the full SCFT. The extent to which fluctuations affect phase behavior increases as the invariant polymerization index, $\bar{N} \equiv N\rho_0^2 a^6$, is decreased. Weakly segregated microstructures are most susceptible to fluctuations, which can destroy long-range order transforming them into the disordered state. To date, fluctuation corrections have been incorporated into both the RPA[21,39,48] and the DFT.[49] The RPA-based calculations examine the vicinity of the mean-field critical point (see Figures 4 and 5) where fluctuations are greatest. They illustrate that fluctuations prevent the critical point from occurring and shift the order–disorder transition (ODT) to larger χN by an amount proportional to $\bar{N}^{-1/3}$. They also open up windows of first-order transitions between the DIS phase and the various ordered structures. In the infinite molecular weight limit, fluctuations are completely suppressed and the mean-field behavior is recovered. The DFT calculation shows that fluctuation effects diminish rapidly as the ordered structures become segregated. Calculations have yet to determine whether fluctuations alter the delicate free energy balance in the complex phase region. Experiments suggest that at weak to intermediate segregations, they can produce significant changes to the order–order phase transitions.[1]

Although the present theoretical result agrees with experiment in that the $Q_{Ia\bar{3}d}$ phase exists as a bubble,[1,11,12] there are some discrepancies in regard to the complex phases. Experiments indicate that, as molecular weight increases, the $Q_{Ia\bar{3}d}$ phase becomes unstable and the only complex phase that appears stable is the HPL one.[1] This discrepancy cannot be attributed to the mean-field approximation, because these are large $\bar{N}$ results for which fluctuation effects are diminished. Although these discrepancies could be a result of nonequilibrium effects in the experiments, it could just as well be due to limitations in the standard model. While this model has proven itself to be rather successful in most regards, the issue of stability among complex phases is a subtle one that may require a more refined approach.

Theoretical research has been based on the underlying assumption that block copolymer phase behavior is reasonably universal and that all AB diblock systems have phase diagrams that are topologically equivalent to that of the standard model. Considering the close competition of the complex phases in the region between the L and H phases, this is unlikely. Presumably, refinements to the model will alter the subtle balance of energies between the complex phases. Although consideration of conformational asymmetry between the A and B blocks[50,51] has not yet produced qualitatively different behavior,[3] some of our calculations have indicated that high asymmetries may cause the HPL phase to become stable. It is possible that polydispersity could alter the phase diagram. Even though this has been incorporated into the RPA,[52] there is little information regarding its effect on the phase boundaries. However, SCFT calculations illustrate that binary blends of closely matched diblocks behave like a monodisperse diblock melt with compositionally averaged parameters,[53] strongly suggesting that a moderate polydispersity will have little effect on phase behavior. Another issue worthy of consideration is the relaxation of the incompressibility constraint. Several works[18,54] have illustrated how compressibility effects can be dealt with, and recently it was demonstrated that such equation-of-state effects can produce a temperature dependence of χ that results in a lower critical point.[55] Nevertheless, our preliminary results suggest that compressibility effects have little influence on the phase diagram when plotted in the $\chi N - f$ plane. It may be important to more accurately treat the interactions between A and B segments. For polymer blends, the enthalpy of mixing A and B homopolymers is assumed to be $\chi\phi_A\phi_B$. The fact that the actual enthalpy does not fit this simple form results in a χ parameter which depends on ϕ_A. In block copolymer melts where ϕ_A is not a simple scalar but rather a spatially dependent quantity such a treatment is unsatisfactory. The solution is to examine more general interaction terms.[19] Another issue is the effect of interactions with a finite range. Helfand *et al.*[18] have illustrated how this can be incorporated into the theory. Still, another concern is the effect of finite persistence lengths. The wormlike model[70] offers a way in which this can be included into the present calculation.[71] With the study of refinements like those discussed here, our understanding of what favors the occurrence of complex phases will no doubt become more complete.

Acknowledgment. We are grateful to D. A. Hajduk and M. A. Hillmyer for a critical reading of the manuscript. This work has been supported by the University of Minnesota Supercomputer Institute and by the National Science Foundation (DMR 94-05101).

References and Notes

(1) Bates, F. S.; Schulz, M. F.; Khandpur, A. K.; Förster, S.; Rosedale, J. H.; Almdal, K.; Mortensen, K. *Faraday Discuss.* **1994**, *98*, 7.
(2) Bates, F. S.; Fredrickson, G. H. *Annu. Rev. Chem.* **1990**, *41*, 525.

(3) Matsen, M. W.; Schick, M. *Macromolecules* **1994**, *27*, 4014.
(4) Bates, F. S.; Berney, C. V.; Cohen, R. E. *Macromolecules* **1982**, *15*, 584.
(5) Richards, R. W.; Thomason, J. L. *Macromolecules* **1983**, *16*, 982.
(6) Aggarwal, S. L. *Polymer* **1972**, *17*, 938.
(7) Thomas, E. L.; Alward, D. B.; Kinning, D. J.; Martin, D. C.; Handlin, D. L.; Fetters, L. J. *Macromolecules* **1986**, *19*, 2197.
(8) Hajduk, D. A.; Harper, P. E.; Gruner, S. M.; Honeker, C. C.; Kim, G.; Thomas, E. L. *Macromolecules* **1994**, *27*, 4063.
(9) Schulz, M. F.; Bates, F. S.; Almdal, K.; Mortensen, K. *Phys. Rev. Lett.* **1994**, *73*, 86.
(10) Hamley, I. W.; Koppi, K. A.; Rosedale, J. H.; Bates, F. S.; Almdal, K.; Mortensen, K. *Macromolecules* **1993**, *26*, 5959.
(11) Förster, S.; Khandpur, A. K.; Zhao, J.; Bates, F. S.; Hamley, I. W.; Ryan, A. J.; Bras, W. *Macromolecules* **1994**, *27*, 6922.
(12) Khandpur, A. K.; Förster, S.; Bates, F. S.; Hamley, I. W.; Ryan, A. J.; Bras, W.; Almdal, K.; Mortensen, K. *Macromolecules* **1995**, *28*, 8796.
(13) Hasegawa, H.; Tanaka, H.; Yamasaki, K.; Hashimoto, T. *Macromolecules* **1987**, *20*, 1651.
(14) Spontak, R. J.; Smith, S. D.; Ashraf, A. *Macromolecules* **1993**, *26*, 956.
(15) Hajduk, D. A.; Harper, P. E.; Gruner, S. M.; Honeker, C. C.; Kim, G.; Thomas, E. L.; Fetters, L. J. *Macromolecules* **1995**, *28*, 2570.
(16) Helfand, E.; Wasserman, Z. R. *Macromolecules* **1976**, *9*, 879.
(17) Helfand, E.; Wasserman, Z. R. *Macromolecules* **1978**, *11*, 960; **1980**, *13*, 994.
(18) Helfand, E.; Tagami, Y. *Polym. Lett.* **1971**, *9*, 741; *J. Chem. Phys.* **1971**, *56*, 3592; *J. Chem. Phys.* **1972**, *57*, 1812. Helfand, E.; Sapse, A. M. *J. Chem. Phys.* **1975**, *62*, 1327.
(19) Helfand, E. *J. Chem. Phys.* **1975**, *62*, 999.
(20) Leibler, L. *Macromolecules* **1980**, *13*, 1602.
(21) Fredrickson, G. H.; Helfand, E. *J. Chem. Phys.* **1987**, *87*, 697.
(22) Semenov, A. N. *Sov. Phys. JETP* **1985**, *61*, 733.
(23) Ohta, T.; Kawasaki, K. *Macromolecules* **1986**, *19*, 2621.
(24) Anderson, D. M.; Thomas, E. L. *Macromolecules* **1988**, *21*, 3221.
(25) Lescanec, R. L.; Muthukumar, M. *Macromolecules* **1993**, *26*, 3908.
(26) Melenkevitz, J.; Muthukumar, M. *Macromolecules* **1991**, *24*, 4199.
(27) McMullen, W. E. *Macromolecules* **1993**, *26*, 1027.
(28) Vavasour, J. D.; Whitmore, M. D. *Macromolecules* **1992**, *25*, 5477.
(29) Olvera de la Cruz, M.; Mayes, A. M.; Swift, B. W.; *Macromolecules* **1992**, *25*, 944.
(30) Hamley, I. W.; Bates, F. S. *J. Chem. Phys.* **1994**, *100*, 6813.
(31) Matsen, M. W.; Schick, M. *Phys. Rev. Lett.* **1994**, *72*, 2660.
(32) Fredrickson, G. H. *Macromolecules* **1991**, *24*, 3456.
(33) Olmsted, P. D.; Milner, S. T. *Phys. Rev. Lett.* **1994**, *72*, 936; **1995**, *74*, 829. Milner, S. T. *J. Polymer Sci. B* **1994**, *32*, 2743.
(34) Likhtman, A. E.; Semenov, A. N. *Macromolecules* **1994**, *27*, 3103.
(35) Matsen, M. W.; Bates, F. S. *Macromolecules* **1995**, *28*, 8884.
(36) Mayes, A. M.; Olvera de la Cruz, M. *Macromolecules* **1991**, *24*, 3975.
(37) Shull, K. R. *Macromolecules* **1992**, *25*, 2122.
(38) Sones, R. A.; Terentjev, E. M.; Petschek, R. G. *Macromolecules* **1993**, *26*, 3344.
(39) Barrat, J.-L.; Fredrickson, G. H. *J. Chem. Phys.* **1991**, *95*, 1281. Mayes, A. M.; Olvera de la Cruz, M. *J. Chem. Phys.* **1991**, *95*, 4670.
(40) Semenov, A. N. *Macromolecules* **1993**, *26*, 6617; see ref 21 within.
(41) Shull, K. R.; Mayes, A. M.; Russell, T. P. *Macromolecules* **1993**, *26*, 3929.
(42) Semenov, A. N. *Macromolecules* **1989**, *22*, 2849.
(43) Semenov, A. N. *Macromolecules* **1993**, *26*, 2273.
(44) Ball, R. C.; Marko, J. F.; Milner, S. T.; Witten, T. A. *Macromolecules* **1991**, *24*, 693. Li, H.; Witten, T. A. *Macromolecules* **1994**, *27*, 449.
(45) Fredrickson, G. H. *Macromolecules* **1993**, *26*, 4351.
(46) Matsen, M. W.; Whitmore, M. D. *Macromolecules*, submitted.
(47) Matsen, M. W. *Phys. Rev. Lett.* **1995**, *74*, 4225; *Macromolecules* **1995**, *28*, 5765.
(48) Dobrynin, A. V.; Erukhimovich, I. Ya. *J. Phys. II Fr.* **1991**, *1*, 1387.
(49) Muthukumar, M. *Macromolecules* **1993**, *26*, 5259.
(50) Vavasour, J. D.; Whitmore, M. D. *Macromolecules* **1993**, *26*, 7070.
(51) Matsen, M. W.; Schick, M. *Macromolecules* **1994**, *27*, 6761.
(52) Leibler, L.; Benoit, H. *Polymer* **1983**, *22*, 195. Hong, K. M.; Noolandi, K. M. *Polymer Commun.* **1984**, *25*, 265. Benoit, H.; Hadziioannou, G. *Macromolecules* **1988**, *21*, 1449. Burger, C.; Ruland, W.; Semenov, A. N. *Macromolecules* **1990**, *23*, 3339.
(53) Matsen, M. W.; Bates, F. S. *Macromolecules* **1995**, *28*, 7298. Schulz, M. F.; Khandpur, A. K.; Matsen, M. W.; Bates, F. S.; Almdal, K.; Mortensen, K.; Hajduk, D. A.; Gruner, S. M., in preparation.
(54) Hong, K. M.; Noolandi, K. M. *Macromolecules* **1981**, *14*, 1229.
(55) Yeung, C.; Desai, R. C.; Shi, A.-C.; Noolandi, J. *Phys. Rev. Lett.* **1994**, *72*, 1834.
(56) Whitmore, M. D.; Vavasour, J. D. *Acta Polym.*, **1995**, *46*, 341.
(57) Scheutens, J. M. H. M.; Fleer, G. J. *J. Phys. Chem.* **1979**, *83*, 1619; *Macromolecules* **1985**, *18*, 1882.
(58) Brazovskii, S. A. *Sov. Phys. JETP* **1975**, *41*, 85.
(59) Marques, C. M.; Cates, M. E. *Europhys. Lett.* **1990**, *13*, 267.
(60) Hajduk, D. A.; Gruner, S. M.; Rangarajan, P.; Register, R. A.; Fetters, L. J.; Honeker, C. C.; Albalak, R. J.; Thomas, E. L. *Macromolecules* **1994**, *27*, 490.
(61) Unnormalized basis functions can be found in: *International Tables for X-Ray Crystallography*; Henry, N. F. M., Londsdale, K., Eds.; Kynoch: Birmingham, U.K., 1969. Those of the $Q_{Ia\bar{3}d}$ phase appear on pp 524–5.
(62) Fried, H.; Binder, K. *J. Chem. Phys.* **1991**, *94*, 8349; *Europhys. Lett.* **1991**, *16*, 237.
(63) Almdal, K.; Rosedale, J. H.; Bates, F. S.; Wignall, G. D.; Fredrickson, G. H. *Phys. Rev. Lett.* **1990**, *65*, 1112. Foster, M. D.; Sikka, M.; Singh, N.; Bates, F. S.; Satija, S. K.; Makrzak, C. F. *J. Chem. Phys.* **1992**, *96*, 8605.
(64) Hadziioannou, G.; Skoulios, A. *Macromolecules* **1982**, *15*, 258.
(65) Hashimoto, T.; Shibayama, M.; Kawai, H. *Macromolecules* **1980**, *13*, 1237.
(66) Alexander, S.; McTague, J. *Phys. Rev. Lett.* **1978**, *41*, 708.
(67) Disko, M. M.; Liang, K. S.; Behal, S. K.; Roe, R. J.; Jeon, K. J. *Macromolecules* **1993**, *26*, 2983.
(68) For the L phase, the lamellar spacing is $2\pi/q^*$, for the $Q_{Ia\bar{3}d}$ phase, the size of the unit cell is $2\pi 6^{1/2}/q^*$, for the H phase, the spacing between the cylinders is $4\pi/3^{1/2}q^*$, and for both the bcc and fcc lattices, the spacing between the spheres is $\pi 6^{1/2}/q^*$.
(69) Koppi, K. A.; Tirrell, M.; Bates, F. S.; Almdal, K.; Mortensen, K. *J. Rheol.* **1994**, *38*, 999.
(70) Morse, D. C.; Fredrickson, G. H. *Phys. Rev. Lett.* **1994**, *73*, 3235. Schmid, F.; Müller, M. *Macromolecules* **1995**, *28*, 8639.
(71) Matsen, M. W. *J. Chem. Phys.*, submitted.

MA951138I